Hydration/Dehydration and Cation Migration Processes at High Temperature in Zeolite Chabazite

M. Zema,*[,†,‡] S. C. Tarantino,[†] and G. Montagna[†,§]

Dipartimento di Scienze della Terra, Università di Pavia, Via Ferrata 1, 27100 Pavia, Italy, and CNR-IGG, Sezione di Pavia, Via Ferrata 1, 27100 Pavia, Italy

Received March 17, 2008. Revised Manuscript Received June 20, 2008

High temperature structural behavior of a natural chabazite of composition $(Ca_{1.1}Na_{0.4}K_{0.7})$-$[Si_{8.6}Al_{3.4}O_{24}]\cdot 14.4H_2O$ has been characterized by means of in situ HT single-crystal X-ray diffraction (SC-XRD) and thermogravimetric analysis. Lattice dimensions have been measured in the 25−700 °C range and crystal structure refined from XRD data collected at $T = 25$, 100, 125, 175, 250, 300, 425, and 600 °C. Variations of unit-cell parameters as a function of temperature reveal two discontinuities at 100 and 200 °C, to which no symmetry changes are associated, and an overall volume reduction of 2.8%. Between 200 and 250 °C, a steep contraction of cell volume is associated with a significant broadening of diffraction profiles, which turn sharp and narrow at higher temperatures. As the dehydration process proceeds with increasing T, cationic sites partly coordinated by extraframework water molecules become unstable and cations migrate toward new positions. Cations occupying the C2, C3, and C4 sites at room temperature move first toward C2 while T is raised to 200 °C, and for $T > 200$ °C they start migrating toward smaller cavities where coordination is assured by oxygen atoms of the framework only, the six-membered double ring (C1 site), and a peripheral position within the eight-membered ring. The latter position has been labeled as C5. Sites C1 and C5 are stable up to 700 °C. Reversal experiments demonstrated that the whole process is reversible under the conditions of this study; by decreasing temperature, water enters the structure again and cations migrate back to their original positions.

1. Introduction

Chabazite, with ideal composition $(Ca_{0.5},Na,K)_4$-$[Al_4Si_8O_{24}]\cdot 12H_2O$, is one of the most widespread natural zeolites and one of the first zeolites to be studied for its excellent ion-exchange properties and for the wide range of its industrial and technological applications. The so-called "chabazite cage", typical of this structure, is depicted in Figure 1. It shows a framework structure (framework type CHA) consisting of parallel stacks of six-membered double rings (*d*6*R*) in the sequence ABC. The largest channels, perpendicular to [001] (hexagonal setting), are confined by eight-membered rings. Chabazite is rhombohedral $R\bar{3}m$, with unit-cell parameters $a_H \approx 13.7-13.9$ Å, $c_H \approx 14.8-15.4$ Å in the hexagonal setting.[1,2] This space group implies a fully disordered Si−Al distribution and is only a pseudo space group of chabazite.[3] Because of some Si−Al ordering in the six independent (in $P\bar{1}$) tetrahedra, there is in fact a deviation from the trigonal toward the triclinic symmetry.[4,5] However, this ordering appears to be rather random as due to randomly arranged domains with perfect Si−Al ordering. Passaglia gave a thorough description of the chemical variability of natural chabazites and of the relations between chemical composition and physical properties.[6] Since the pioneering works of Ames,[7,8] a series of cation-exchange experiments (Na, K, Ag, Cs, Ca, Sr, Ba, Cd, Mn, Co, Cu, NH_4^+) were carried out.[9−14] Accurate determinations of the positions of extraframework cations and water molecules in the crystal structure of natural and cation-exchanged hydrated chabazites at room temperature have been given by Alberti et al.[15] and Calligaris et al.[16]

The response of zeolites to changes in T and/or vapor pressure is a very important aspect of their behavior and has an impact on their industrial applications. For instance, they are used as catalysts at high temperature, and the dynamics

* Corresponding author. Telephone: +39 0382 985869. Fax: +39 0382 985890. E-mail: michele.zema@unipv.it.
† Università di Pavia.
‡ CNR-IGG.
§ Present address: Dipartimento di Scienze della Terra, Università di Modena e Reggio Emilia, Largo S. Eufemia 19, 41100 Modena, Italy.

(1) Dent, L. S.; Smith, J. V. *Nature* **1958**, *181*, 1794.
(2) Smith, J. V.; Rinaldi, F.; Dent Glasser, L. S. *Acta Crystallogr.* **1963**, *16*, 45.
(3) Smith, J. V.; Knowles, C. R.; Rinaldi, F. *Acta Crystallogr.* **1964**, *17*, 374.
(4) Mazzi, F.; Galli, E. *N. Jb. Miner. Mh.* **1983**, *10*, 461.
(5) Engelhardt, G.; Michel, D. *High Resolution Solid-State NMR of Silicates and Zeolites*; John Wiley & Sons: Chichester, UK, 1987.
(6) Passaglia, E. *Am. Mineral.* **1970**, *55*, 1278.
(7) Ames, L. L., Jr. *Am. Mineral.* **1964**, *49*, 127.
(8) Ames, L. L., Jr. *Am. Mineral.* **1964**, *49*, 1099.
(9) Smith, J. V. *Chem. Rev.* **1988**, *88*, 149.
(10) Dyer, A.; Zubair, M. *Microporous Mesoporous Mater.* **1998**, *22*, 135.
(11) Shim, S. H.; Navrotsky, A.; Gaffney, T. R.; MacDougall, J. E. *Am. Mineral.* **1999**, *84*, 1870.
(12) Moroz, N. K.; Seryotkin, Yu. V.; Afanassyev, I. S.; Bakakin, V. V. *J. Struct. Chem.* **2002**, *43*, 595.
(13) Seretkin, Yu. V.; Bakakin, V. V.; Belitzkii, I. A. *J. Struct. Chem.* **2005**, *46*, 659.
(14) Gualtieri, A. F.; Passaglia, E. *Eur. J. Mineral.* **2006**, *18*, 351.
(15) Alberti, A.; Galli, E.; Vezzalini, G.; Passaglia, E.; Zanazzi, P. F. *Zeolites* **1982**, *2*, 303.
(16) Calligaris, M.; Nardin, G.; Randaccio, L.; Chiaramonti, P. C. *Acta Crystallogr., Sect. B* **1982**, *38*, 602.
(17) Woodcock, D. A.; Lightfood, P.; Villaescusa, L. A.; Diaz-Cabanas, M. J.; Camblor, M. A.; Engberg, D. *Chem. Mater.* **1999**, *11*, 2508.

10.1021/cm800781t CCC: $40.75
Published on Web 08/21/2008

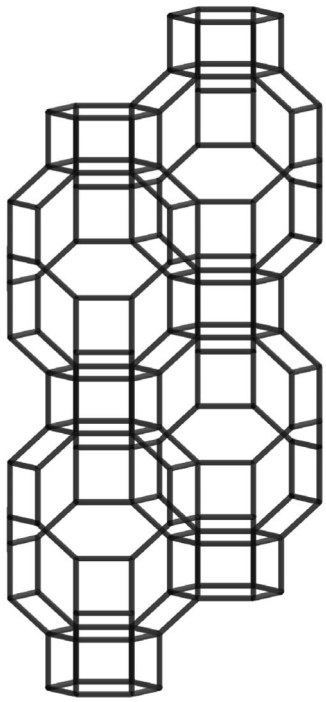

Figure 1. The chabazite cage. Solid lines represent T−O−T linkages.

of the structure can affect the reaction mechanism and the transport of cations or molecules within the pores/cage. The high temperature behavior of zeolite chabazite is particularly interesting because chabazite has the largest negative thermal expansion (NTE) coefficient known in aluminosilicates (see ref 17 and references therein). The mechanism of this phenomenon is still unclear; on the one hand, Hammonds et al. explained it in terms of the presence of rigid unit modes (RUMs).[18] On the other hand, more recently, Martinez-Iñesta and Lobo, using the pair distribution function (PDF) method, proposed a new mechanism of contraction of chabazite with temperature, which involves distortion of the tetrahedra.[19]

For what concerns the thermal hydration−dehydration behavior, chabazite belongs to category-1 in the classification of Alberti and Vezzalini based on the volumetric and structural effects of heating, and hence it should be characterized by reversible dehydration accompanied by rearrangement of the extraframework cations and residual water molecules with little modification of the framework and unit-cell volume.[20] Following Baur, the chabazite framework may be classified as "noncollapsible".[21] Finally, the stability index (SI) of chabazite, as defined by Cruciani, is 5, indicating thermal stability up to ca. 800 °C.[22] The crystal structures of dehydrated forms of chabazite were determined by Smith et al.,[23] Mortier et al.,[24] Butikova et al.[25] (Ca-chabazite), and Mortier et al.[26] (Na-chabazite). Measurements of dehydration thermodynamics of natural and cation-exchanged chabazite have been performed by several authors[11,27−29] and were reviewed by Fialips at al., who revealed the existence of three energetically distinct types of H_2O, which are lost at different stages during dehydration by means of isobaric thermogravimetric measurements.[30] The occurrence of a phase transition at a certain stage of dehydration (ca. 3.8 mol of H_2O per unit-cell) has been also reported on the basis of thermochemical data.[28,29] Such differences in hydration energetics might be due to different cation sites occupancies and therefore different binding of H_2O within the framework. A thorough understanding of the linked structural changes and H_2O incorporation processes can be rationalized by comparing the thermodynamic description to a full structural characterization of these processes.

In the present work, the modifications of the CHA framework at high temperature have been characterized by means of in situ single-crystal X-ray diffraction, thus allowing to elucidate the structural mechanisms of the dehydration/hydration and cation migration processes.

2. Experimental Section

2.1. Sample. A natural chabazite sample from Talisker Bay, Skye Island (Scotland), has been used for the present work. The SC-XRD study was carried out on sample CHA Tal N.3, which has dimensions 0.14 × 0.14 × 0.25 mm, and shows very narrow and steep diffraction profiles. A second crystal of similar size, labeled CHA Tal N.8, was used to check the reproducibility of the experiment. For the thermogravimetric study, 5.31 mg of powdered sample was used.

2.2. Electron Microprobe Analysis. Chemical analysis of the same single crystals as used for X-ray diffraction experiments was performed at the Department of Earth Sciences of University of Modena with a ARL-SEMQ electron microprobe operating in the wavelength dispersive (WDS) mode. Standards used were: Amelia albite for Si, Al, and Na, asbestos microcline for K, paracelsian for Ba, and synthetic diopside Di85-JD15, AN70 glass, Sr-anorthite, and P140 olivine for Mg, Ca, Sr, and Fe, respectively. X-ray counts were converted into oxide weight percentages using the PROBS correction program.[31] For most zeolites, in particular those with large channels, the electron bombardment and vacuum conditions in the microprobe sample chamber cause a loss of H_2O and extraframework cation migration. To minimize these effects, a beam current of 20 nA and a defocused beam of 15 μm and short counting times (5, 10, and 5 s on high background, peak, and low background, respectively) were used. Analyses are precise to within 1% for major elements and 3−5% for minor elements. The analysis and the formula calculated on the basis of 24 oxygen atoms are given in Table 1.

2.3. Thermogravimetric Analysis. Isothermal gravimetric and thermogravimetric (TG) measurements in the temperature range 25−800 °C were performed with a 951 Thermogravimetric

(18) Hammonds, K. D.; Heine, V.; Dove, M. T. *J. Phys. Chem. B* **1998**, *102*, 1759.
(19) Martinez-Iñesta, M. M.; Lobo, R. F. *J. Phys. Chem. B* **2005**, *109*, 9389.
(20) Alberti, A.; Vezzalini, G. In *Proc. Sixth Int'l Zeolite Conf.*; Olson, D., Bisio, A., Eds.; Betterworths: Guilford, UK, 1984; pp 834−841.
(21) Baur, W. H. *J. Solid State Chem.* **1992**, *97*, 243.
(22) Cruciani, G. *J. Phys. Chem. Solids* **2006**, *67*, 1973.
(23) Smith, J. V. *Acta Crystallogr.* **1962**, *15*, 835.
(24) Mortier, W. J.; Pluth, J. J.; Smith, J. V. *Mater. Res. Bull.* **1977**, *12*, 97.
(25) Butikova, I. K.; Shepelev, Yu. F.; Smolin, Yu. I. *Kristallografiya* **1993**, *38*, 68.
(26) Mortier, W. J.; Pluth, J. J.; Smith, J. V. *Mater. Res. Bull.* **1977**, *12*, 241.
(27) Drebushchak, V. A. *J. Therm. Anal. Calorim.* **1999**, *58*, 653.
(28) Valueva, G. P. *Geokhimiya* **1990**, *1*, 130.
(29) Valueva, G. P.; Goryainov, S. V. *Geol. Geofiz.* **1992**, *12*, 81.
(30) Fialips, C. I.; Carey, J. W.; Bish, D. L. *Geochim. Cosmochim. Acta* **2005**, *69*, 2293.
(31) Donovan, J. J.; Rivers, M. L. *Microbeam Anal.* **1990**, 66.

Table 1. Chemical Composition of Sample CHA Tal N.3[a]

oxides (wt %)	
K_2O	3.7(6)
CaO	6.8(2)
Na_2O	1.3(2)
SiO_2	58.5(8)
Al_2O_3	19.5(5)
totals	89.8(5)
a.p.f.u. based on 24 oxygen atoms	
K	0.7(1)
Ca	1.08(3)
Na	0.37(7)
Si	8.64(3)
Al	3.39(6)
totals	14.2(1)
Si+Al	12.03(6)
Si/Al	2.55(5)
Ca+Na+K	2.2(2)
extraframework charge	3.2(2)
cation-framework charge	−0.2(2)
no. of spot analyses	4

[a] Standard deviations are given in parentheses.

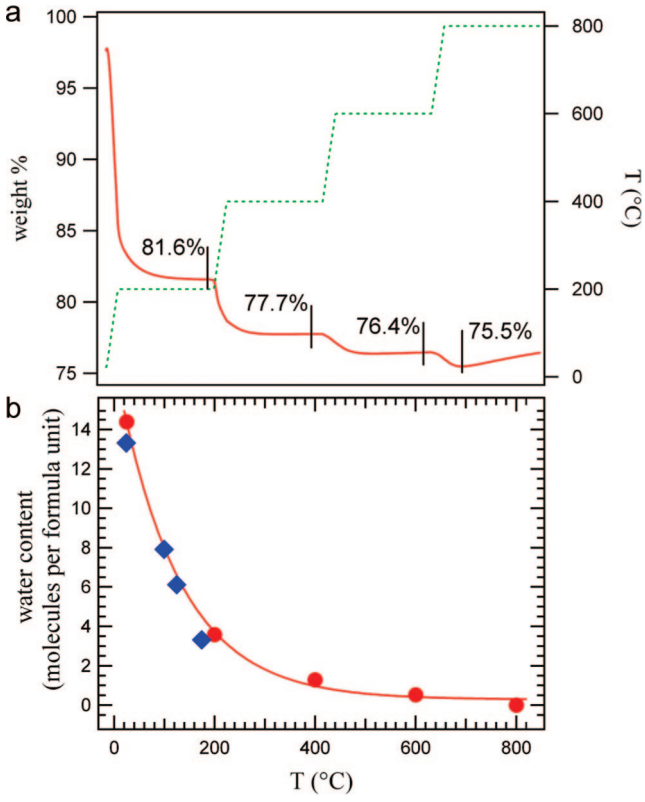

Figure 2. (a) TG curve for the chabazite sample. Dashed line shows the temperature evolution during the experiment (right axis). Initial weight: 5.31 mg. (b) Water content in chabazite as determined by TG analysis (●) and structure refinements (◆). Exponential fit through data from TG analysis is also reported.

Analyzer attachment of a TA 2000 thermal analysis system, using a platinum sample holder. The measurements were carried out on 5.31 mg of powdered sample in air under static conditions. The heating rate was 5 °C/min, and 5 h long isotherms were recorded every 200 °C. The resulting TG curve is reported in Figure 2a.

2.4. Room-Temperature SC-XRD Data Collections. Intensity data were collected at room temperature on the untreated crystal and at the end of the high temperature study. Data collections were carried out using a Bruker AXS SMART-Apex diffractometer equipped with a CCD detector. Operating conditions were 50 kV and 30 mA. The Bruker SMART system of programs was used for preliminary crystal lattice determination and X-ray data collection. A total of 3360 frames (resolution: 512 × 512 pixels) were collected with four different goniometer settings using the ω scan mode (scan width, 0.2° ω; exposure time, 10 s/frame; detector−sample distance, 4 cm). Completeness of measured data was achieved up to 38.4° θ. The Bruker program SAINT+ was used for data reduction including intensity integration, background, and Lorentz-polarization corrections. Final unit-cell parameters (Table 2) were obtained by a least-squares procedure based on the positions of all measured reflections. These values are in good agreement with those gained by the conventional diffractometer (see Table 3), within the uncertainties of both sets of measurements. The semiempirical absorption correction of Blessing,[32] based on the determination of transmission factors for equivalent reflections, was applied using the program SADABS.[33] Details on CCD data collections at room temperature are reported in Table 2.

2.5. Measurement of Unit-Cell Parameters at High Temperature. Unit-cell parameters of crystal CHA Tal N.3 were measured by in situ SC-XRD in the temperature range 25−600 °C. The measurements were performed using a conventional Philips PW 1100 four-circle diffractometer equipped with a microfurnace for in situ high-temperature experiments. Operating conditions were 55 kV and 30 mA, with Mo Kα ($\lambda = 0.71073$ Å) incident radiation. Horizontal and vertical apertures were 2.0° and 1.5°, respectively. At each working temperature, lattice parameters were preliminarily measured by centring 26 reflections in the range $11.4° \leq 2\theta \leq 31.2°$. Unit-cell parameters were accurately derived, at intervals of 25 °C, from a least-squares procedure based on the Philips LAT routine taking into account 40 d^*-spacings, each measured considering all of the reflections in the range $3° > \theta > 26.5°$, and are reported in Table 3 both in the hexagonal and in the rhombohedral settings. The reversibility of the process was checked by measuring lattice parameters while the crystal was cooled from 600 °C to room temperature.

A sensible variation of diffraction profiles width was noticed during the heating experiment; for this reason, eight reflections characterized by relatively high intensity and spread on different classes (003, 009, 030, 090, 300, 900, $\bar{1}14$, $04\bar{1}$, $\bar{6}3\bar{3}$ in the hexagonal setting) were scanned by $\omega-2\theta$ scan mode (scan width, 2.0° ω; scan speed, 0.05° ω/s) during reversal experiment and fitted using Voigt profiles with the MultiPeakFitting routine from IGOR Pro software (Wavemetrics, Inc., OR). All reflections behaved similarly with decreasing temperature; hence the fwhm values of only one reflection ($04\bar{1}$) as a function of T are reported in Table 4.

Unit-cell parameters of crystal CHA Tal N.8 were measured by the reflections centring procedure only. The experiment was carried out in the temperature range from room temperature to 700 °C both under "heating" and "cooling" conditions. Because all of the values obtained on this crystal are superimposable to those of crystals N.3, they are not reported in tables. In this case, the same diffraction profiles analyzed on sample N.3 were recorded during the heating experiment. The similarity in the peak width variation of all of the analyzed reflections was again confirmed; therefore, fitting results on reflection $04\bar{1}$ only are reported in Table 4.

2.6. High-Temperature SC-XRD Data Collections. Diffracted intensities were collected at 25°, 100°, 125°, 175°, 250°, 300°, 425°, and 600 °C on crystal CHA Tal N.3 by the Philips PW1100 diffractometer using the same operating conditions as reported above. All reflections with general indexes hkl, $\bar{h}kl$, $h\bar{k}l$, and $\bar{h}\bar{k}l$ in the hexagonal setting (starting from 250 °C only hkl and $\bar{h}kl$) were

(32) Blessing, R. H. *Acta Crystallogr., Sect. A* **1995**, *51*, 33.
(33) Sheldrick, G. M. *SADABS*; University of Göttingen: Germany, 2003.

Table 2. Details on Room Temperature Data Collections on Crystal CHA Tal N.3[a]

	untreated	after HT treatment
a_R (Å)	9.4034(5)	9.4056(4)
α_R (deg)	94.32(1)	94.29(1)
V_R (Å^3)	824.0(1)	824.70(9)
D_{calc} (g cm^{-3})	2.11	2.11
μ (mm^{-1})	0.858	0.857
T_{min}/T_{max}	0.903	0.855
θ range (deg)	2.2−38.3 (completeness 99.0%)	2.2−38.2 (completeness 98.4%)
index ranges	$-16 \le h \le 16$, $-16 \le k \le 16$, $-16 \le l \le 16$	$-16 \le h \le 16$, $-16 \le k \le 16$, $-16 \le l \le 16$
reflns measured	62 013 (16 171 after merging identical reflns)	61 617 (16 130 after merging identical reflns)
R_{int}[b]	0.0483 (1660 unique reflns)	0.0446 (1646 unique reflns)
R_1[c]	0.0475 (1520 reflns with $I > 2\sigma_I$)	0.0565 (1530 reflns with $I > 2\sigma_I$)
R_{all}	0.0511	0.0601
wR_2	0.1452	0.1498
GOF[d]	1.087	1.120
refined parameters	70	66
weighting scheme	$w = 1/[\sigma^2(F_o^2) + (0.07\ P)^2 + 0.70\ P]$, where $P = (F_o^2 + 2F_c^2)/3$	$w = 1/[\sigma^2(F_o^2) + (0.07\ P)^2 + 1.12\ P]$, where $P = (F_o^2 + 2F_c^2)/3$
$(\text{shift/e.s.d.})_{max}$	0.001	0.000
max, min $\Delta\rho$ (e$^-$ Å^{-3})	0.85, −0.65	0.81, −0.57

[a] Standard deviations are given in parentheses. [b] $R_{int} = \sum|F_o^2 - \bar{F}_o^2|/\sum F_o^2$. [c] $R_1 = \sum||F_o| - |F_c||/\sum|F_o|$. [d] GOF $= S = \sqrt{(\sum w(F_o^2 - F_c^2)^2/(n-p))}$, where n is the number of reflections and p is the total number of parameters refined.

Table 3. Unit-Cell Parameters of Crystal CHA Tal N.3 Measured in the Range from Room Temperature to 600 °C by Means of the LAT Procedure[a]

	hexagonal setting			rhombohedral setting		
T (°C)	a_H (Å)	c_H (Å)	V_H (Å^3)	a_R (Å)	α_R (deg)	V_R (Å^3)
rt	13.802(2)	15.008(4)	2475.8(9)	9.409	94.35	825.3
50	13.780(1)	14.983(4)	2464.0(9)	9.394	94.36	821.3
75	13.757(3)	14.957(5)	2451.4(12)	9.378	94.36	817.1
100	13.734(3)	14.934(5)	2439.6(12)	9.363	94.35	813.2
125	13.701(2)	15.004(2)	2439.1(8)	9.359	94.11	813.0
125[b]	13.696(2)	15.003(3)	2437.3(8)	9.356	94.10	812.4
125[b]	13.696(2)	15.005(3)	2437.4(9)	9.356	94.09	812.5
125[b]	13.697(2)	15.002(3)	2437.5(8)	9.357	94.10	812.5
150	13.676(2)	15.061(3)	2439.5(11)	9.357	93.91	813.1
175	13.655(3)	15.133(3)	2443.8(11)	9.360	93.69	814.6
200	13.627(3)	15.214(3)	2446.5(11)	9.360	93.42	815.5
225	13.517(3)	15.410(4)	2438.3(14)	9.343	92.67	812.8
250	13.378(3)	15.604(2)	2418.5(13)	9.312	91.83	806.2
275	13.342(3)	15.646(2)	2411.9(12)	9.302	91.63	804.0
300	13.325(3)	15.666(2)	2409.0(12)	9.298	91.54	803.0
325	13.320(3)	15.681(1)	2409.4(11)	9.298	91.49	803.1
350	13.315(3)	15.688(2)	2408.6(11)	9.300	91.47	802.9
375	13.312(3)	15.687(2)	2407.6(13)	9.296	91.45	802.5
400	13.308(3)	15.693(2)	2406.9(11)	9.295	91.43	802.3
425	13.306(3)	15.698(2)	2407.0(10)	9.295	91.41	802.3
450	13.305(3)	15.697(2)	2406.3(12)	9.294	91.41	802.1
475	13.305(3)	15.695(2)	2406.1(11)	9.294	91.42	802.0
500	13.304(3)	15.698(2)	2406.2(11)	9.294	91.41	802.1
550	13.306(3)	15.694(2)	2406.3(11)	9.294	91.42	802.1
600	13.306(3)	15.693(2)	2406.3(11)	9.294	91.42	802.1

[a] Standard deviations are given in parentheses. [b] 90 min after previous measurement.

Table 4. Full Width at Half-Maximum of Reflection 04$\bar{1}$

T (°C)	fwhm (deg)	T (°C)	fwhm (deg)
direct experiment (CHA Tal N.8)		reversal experiment (CHA Tal N.3)	
rt	0.12	600	0.12
50	0.12	500	0.12
100	0.12	400	0.12
150	0.13	300	0.12
200	0.10	250	0.12
210	0.15	225	0.44
220	0.43	225[a]	0.49
230	0.68	225[a]	0.32
240	0.79	225[a]	0.32
250	0.43	225[a]	0.31
260	0.33	200	0.27
270	0.25	200[a]	0.26
280	0.27	150	0.21
290	0.26	100	0.23
300	0.24	rt	0.23
350	0.27		
400	0.25		
450	0.22		
500	0.21		
550	0.21		
600	0.20		

[a] 15 min after previous measurement.

measured in the $\omega-2\theta$ scan mode in the 2−26.5° θ range. The microfurnace itself limits the analyzable angular region to these values. Three standard reflections were collected every 100 reflections. X-ray diffraction intensities were obtained by measuring step-scan profiles and analyzing them by the σ_I/I method.[34,35] Unit-cell parameters were derived by the Philips LAT routine, as described above. Intensities were corrected for absorption using the semiempirical ψ-scan method.[36] Relevant parameters on data collections performed at high temperature are reported in Table 5.

2.7. Structure Refinements. All structure refinements were carried out in space group $R\bar{3}m$ (rhombohedral setting) using SHELXL-97[37] starting from the model of Alberti et al.[15] The atomic scattering curves were taken from the International Tables for X-ray Crystallography.[38] Equivalent reflections were averaged, and the resulting internal agreement factors R_{int} are reported in Tables 2 and 5 for RT and HT data, respectively. Structure factors were weighted according to $w = 1/[\sigma^2(F_o^2) + (AP)^2 + BP]$, where $P = (F_o^2 + 2F_c^2)/3$, and A and B were chosen for every crystal to produce a flat analysis of variance in terms of F_c^2 as suggested by the program. An extinction parameter x was refined to correct the structure factors according to the equation: $F_o = F_c k[1 + 0.001xF_c^2\lambda^3/\sin 2\theta]^{-1/4}$ (where k is the overall scale factor).

In the first stages of structure refinement of data collected at room temperature by the CCD diffractometer, only framework atoms were inserted in the model and refined with isotropic

(34) Lehman, M. S.; Larsen, F. K. *Acta Crystallogr., Sect. A* **1974**, *30*, 580.
(35) Blessing, R. H.; Coppens, P.; Becker, P. *J. Appl. Crystallogr.* **1974**, *7*, 488.
(36) North, A. C. T.; Phillips, D. C.; Mathews, F. S. *Acta Crystallogr., Sect. A* **1968**, *24*, 351.
(37) Sheldrick, G. M. *SHELX97 - Programs for Crystal Structure Analysis (Release 97-2)*; Institut für Anorganische Chemie der Universität: Göttingen, Germany, 1998.
(38) Ibers, J. A.; Hamilton, W. C. *International Tables for X-ray Crystallography, Vol. 4*; Kynoch Press: Birmingham, 1974; pp 99−101.

Table 5. Details on Data Collections and Structure Refinement of Crystal CHA Tal N.3 at Different Temperatures[a]

T (°C)	I_{tot}	I	I_{R1}	R_{int} %	R_1 %	R_{all} %	wR %	S	refined parameters	max, min e$^-$/Å^3
100	3459	632	421	9.08	5.21	8.89	13.5	1.038	52	0.56, −0.44
125	3464	635	417	8.74	4.48	8.63	12.7	1.079	56	0.44, −0.37
175	3483	639	442	8.06	4.67	7.76	12.8	0.996	53	0.45, −0.38
250	1806	636	422	8.13	5.77	9.76	16.0	1.031	45	0.57, −0.42
300	1807	636	442	6.11	4.12	7.36	9.6	0.985	43	0.32, −0.26
425	1799	633	390	8.53	4.18	9.34	8.4	0.942	47	0.27, −0.26
600	1799	633	356	8.93	4.56	10.63	9.3	0.894	47	0.39, −0.28

[a] I_{tot} = reflns measured; I = unique reflns; I_{R1} = reflns with $I > 2\sigma_I$; other symbols as in Table 2.

displacement parameters and Si/Al ratio constrained on the basis of electron microprobe data. The highest peaks in the ΔF map were located at C2, C3, C4, and W1 positions, which were then inserted in the structural model. Cation affinities for extraframework crystallographic sites at room temperature were deduced on the basis of the crystal structures of cation-exchanged chabazite reported by Alberti et al.[15] Therefore, Ca was allowed to partitionate between all three cationic sites, while Na was constrained on site C4 and K on C2. Such partitioning yielded a composition very close to that obtained by EMPA analysis. In the following cycles of structure refinement, all of the other positions occupied by water molecules were revealed by subsequent ΔF maps and inserted in the model. Finally, all framework atoms (with soft constrain on Si/Al ratio), extraframework cations (with soft constrain on total composition), and W1 and W6 water positions were refined with anisotropic displacement parameters, while all other water positions were refined isotropically. All of these parameters were refined simultaneously. Final difference-Fourier maps were featureless.

Structure refinements of data collected at high temperature were carried out starting from the model obtained at the immediately lower temperature using mixed isotropic/anisotropic models. Careful inspections of subsequent difference-Fourier maps allowed to determine reliable structural models at all of the investigated temperatures. Moreover, water content determined from unconstrained refined occupancies is in all cases in very good agreement with data from thermogravimetric analysis, as evident in Figure 2b.

The values of the conventional agreement indices, R_1 and R_{all}, as well as the goodness of fit (GoF) are reported in Tables 2 and 5 for RT and HT data, respectively. Atomic fractional coordinates, equivalent or isotropic displacement parameters, as well as site occupancies are reported in Table 6. Tetrahedral bond distances and angles together with tetrahedral distortion parameters are reported in Table 7, whereas cation−oxygen bond distances are in Table 8. Finally, relevant geometrical parameters for the six-membered and the eight-membered rings of the chabazite cage are reported in Table 9.

3. Results and Discussion

3.1. Thermal Stability and Water Content. In Figure 2a, the thermogravimetric curve obtained in the range from room temperature to 800 °C is depicted. It shows that dehydration starts immediately as soon as the temperature is raised and at all of the isothermal stages at 200, 400, and 600 °C the measured weight reaches a plateau. This clearly indicates that the water content in the chabazite sample, under these static atmospheric conditions, depends exclusively on temperature and hence the hydration/dehydration process is reversible. At T = 800 °C, soon after a plateau is reached, chabazite starts decomposing. This confirms the results of previous investigations on the thermal stability of this phase (see ref 22 and references therein).

The total weight loss of 24.5%, combined with the data obtained from the electron microprobe, yields a chemical formula for the studied chabazite of $(Ca_{1.1}Na_{0.4}K_{0.7})$-$[Si_{8.6}Al_{3.4}O_{24}]\cdot 14.4H_2O$ (considering the sample as fully dehydrated at 800 °C). Water content calculated at the various isothermal stages is reported in Figure 2b as a function of temperature where it is compared with data from structure refinements.

3.2. Variations of Unit-Cell Parameters. Variations of unit-cell parameters and cell volume with temperature are reported in Figure 3 for sample CHA Tal N.3. The hexagonal setting is used here, being more meaningful in terms of the structure itself, because c_H and a_H correspond to length and width of the chabazite channel, respectively. In the T range investigated, chabazite shows an overall cell volume reduction of 2.8%, which is a consequence of a noncontinuous behavior. The process can be conveniently described by dividing it into four steps:

(1) Room temprature to 100 °C: Chabazite shows linear contraction of both a_H and c_H and, consequently, of cell volume.

A first discontinuity occurs at T = 100 °C.

(2) 100−200 °C: The c_H dimension expands in this temperature range, whereas the a_H parameter continues decreasing even showing a slight change of slope at T = 100 °C. The resulting cell volume also shows a discontinuity at 100 °C, and increases from 100 to 200 °C.

A second discontinuity occurs at T = 200 °C.

(3) 200−250 °C: In this range, a steep contraction of cell volume is associated with a significant broadening of diffraction profiles, as shown in Figure 4, where the fwhm of reflection $04\bar{1}$ is reported as a function of temperature. The same behavior shown in figure was displayed by all of the analyzed reflections. Therefore, preferential directions for peak broadening might be excluded. Individual lattice parameters still show opposite behavior in this T range, with a_H parameter continuing decreasing and c_H dimension continuing increasing. A change of slope at T = 200 °C in both cell dimensions variations, which become steeper, is evident from Figure 3.

(4) 250−700 °C: At $T \geq$ 250 °C, diffraction profiles are again sharp and narrow (see Figure 4) and thermal expansion is nil up to 700 °C (in Figure 3 only data obtained in the range from room temperature to 600 °C on crystal CHA Tal N.3 are reported; such behavior has indeed been confirmed on crystal CHA Tal N.8, which has been heated to 700 °C). No significant change is in fact observed in this temperature

(39) Robinson, K.; Gibbs, G. V.; Ribbe, P. H. *Science* **1971**, *172*, 567.
(40) Busing, W. R.; Levy, H. A. *Acta Crystallogr.* **1964**, *17*, 142.

Table 6. Atomic Fractional Coordinates (Rhombohedral Setting), Displacement Factors, and Site Occupancies for Crystal CHA Tal N.3 at Different Temperatures[a]

		rt	100 °C	125 °C	175 °C	250 °C	300 °C	425 °C	600 °C	rt[b]
T 12*i*	*x/a*	0.1045(1)	0.1045(1)	0.1036(1)	0.1021(1)	0.0937(1)	0.0929(1)	0.0926(1)	0.0928(1)	0.1043(1)
	y/b	0.3331(1)	0.3333(1)	0.3318(1)	0.3315(1)	0.3288(1)	0.3287(1)	0.3290(1)	0.3291(1)	0.3330(1)
	z/c	0.8762(1)	0.8765(1)	0.8757(1)	0.8728(1)	0.8624(1)	0.8605(1)	0.8598(1)	0.8596(1)	0.8760(1)
	U_{eq}	0.0113(1)	0.0181(4)	0.0203(4)	0.0219(4)	0.0298(5)	0.0205(3)	0.0233(3)	0.0276(3)	0.0121(1)
O1 6*f*	*x/a*	0.2627(2)	0.2619(4)	0.2635(4)	0.2671(4)	0.2874(4)	0.2900(3)	0.2912(3)	0.2911(3)	0.2631(2)
	y/b	−0.2627(2)	−0.2619(4)	−0.2635(4)	−0.2671(4)	−0.2874(4)	−0.2900(3)	−0.2912(3)	−0.2911(3)	−0.2631(2)
	z/c	0	0	0	0	0	0	0	0	0
	U_{eq}	0.0338(6)	0.046(1)	0.047(1)	0.048(1)	0.039(1)	0.0373(9)	0.039(1)	0.046(1)	0.0332(5)
O2 6*g*	*x/a*	0.1517(2)	0.1519(3)	0.1458(3)	0.1429(4)	0.1224(4)	0.1215(3)	0.1217(3)	0.1231(3)	0.1513(2)
	y/b	−0.1517(2)	−0.1519(3)	−0.1458(3)	−0.1429(4)	−0.1224(4)	−0.1215(3)	−0.1217(3)	−0.1231(3)	−0.1513(2)
	z/c	1/2	0.5	0.5	0.5	0.5	0.5	0.5	0.5	0.5
	U_{eq}	0.0269(5)	0.037(1)	0.042(1)	0.047(1)	0.045(1)	0.0416(9)	0.045(1)	0.054(1)	0.0276(4)
O3 6*h*	*x/a*	0.2530(2)	0.2536(4)	0.2526(4)	0.2491(4)	0.2464(4)	0.2454(3)	0.2440(3)	0.2435(3)	0.2525(2)
	y/b	0.2530(2)	0.2536(4)	0.2526(4)	0.2491(4)	0.2464(4)	0.2454(3)	0.2440(3)	0.2435(3)	0.2525(2)
	z/c	0.8926(3)	0.8948(6)	0.8940(6)	0.8922(6)	0.8692(6)	0.8661(4)	0.8655(4)	0.8659(5)	0.8924(3)
	U_{eq}	0.0317(6)	0.046(1)	0.053(1)	0.054(1)	0.040(1)	0.0398(9)	0.046(1)	0.052(1)	0.0315(5)
O4 6*h*	*x/a*	0.0256(2)	0.0276(4)	0.0272(4)	0.0240(4)	−0.0022(4)	−0.0051(3)	−0.0056(3)	−0.0056(3)	0.0250(2)
	y/b	0.0256(2)	0.0276(4)	0.0272(4)	0.0240(4)	−0.0022(4)	−0.0051(3)	−0.0056(3)	−0.0056(3)	0.0250(2)
	z/c	0.3228(3)	0.3227(5)	0.3107(5)	0.3045(6)	0.2654(6)	0.2629(3)	0.2620(3)	0.2642(4)	0.3225(3)
	U_{eq}	0.0294(5)	0.044(1)	0.048(1)	0.051(1)	0.036(1)	0.0309(8)	0.0336(9)	0.039(1)	0.0299(4)
C1 1*a*	*x/a*				0	0	0	0	0	
	y/b				0	0	0	0	0	
	z/c				0	0	0	0	0	
	U				0.04(4)	0.025(2)[c]	0.027(1)[c]	0.03(1)[c]	0.041(1)[c]	
	Ca				0.03(1)	0.79(2)	0.92(1)	0.97(1)	0.97(1)	
C2 2*c*	*x/a*	0.2268(9)	0.228(2)	0.2100(6)	0.195(4)	0.186(1)	0.179(2)	0.163(3)	0.157(4)	0.2259(7)
	y/b	0.2268(9)	0.228(2)	0.2100(6)	0.195(4)	0.186(1)	0.179(2)	0.163(3)	0.157(4)	0.2259(7)
	z/c	0.2268(9)	0.228(2)	0.2100(6)	0.195(4)	0.186(1)	0.179(2)	0.163(3)	0.157(4)	0.2259(7)
	U	0.038(3)[c]	0.15(1)[c]	0.053(2)	0.065(2)	0.058(8)	0.07(1)	0.061(3)	0.07(3)	0.031(2)[c]
	K	0.34(2)	0.36(1)	0.37(1)	0.28(1)	0	0	0	0	0.30(3)
	Ca	0	0.11(1)	0.18(2)	0.45(1)	0.19(1)	0.1011(9)	0.0616(8)	0.043(8)	0
C2a 2*c*	*x/a*		0.211(2)	0.184(2)	0.149(3)					
	y/b		0.211(2)	0.184(2)	0.149(3)					
	z/c		0.211(2)	0.184(2)	0.149(3)					
	U		0.019(6)	0.033(8)	0.045(9)					
	Na		0.19(1)	0.20(1)	0.16(1)					
C3 2*c*	*x/a*	0.4044(4)	0.409(4)							0.4040(3)
	y/b	0.4044(4)	0.409(4)							0.4040(3)
	z/c	0.4044(4)	0.409(4)							0.4040(3)
	U	0.073(5)[c]	0.04(2)							0.074(4)[c]
	Ca	0.12(1)	0.04(1)							0.1(1)
	Na	0.4(2)	0							0.4(2)
C4 6*h*	*x/a*	0.5803(9)	0.579(1)	0.569(4)						0.5803(9)
	y/b	0.5803(9)	0.579(1)	0.569(4)						0.5803(9)
	z/c	0.234(2)	0.230(2)	0.269(6)						0.236(2)
	U	0.074(5)[c]	0.076(8)	0.29(3)						0.096(6)[c]
	Ca	0.125(4)	0.123(8)	0.122(8)						0.129(6)
C5 12*i*	*x/a*					−0.030(5)	−0.023(1)	−0.025(2)	−0.025(3)	
	y/b					0.454(6)	0.459(1)	0.453(1)	0.456(1)	
	z/c					0.454(6)	0.459(2)	0.453(1)	0.456(1)	
	U					0.09(2)	0.107(7)	0.157(9)[c]	0.18(1)[c]	
	K					0.10(3)	0.1453(6)	0.122(5)	0.122(5)	
	Na					0	0	0.09(1)	0.09(1)	
W1 3*d*	*x/a*	0	0	0	0	0				0
	y/b	1/2	1/2	1/2	1/2	1/2				1/2
	z/c	1/2	1/2	1/2	1/2	1/2				1/2
	U	0.142(9)[c]	0.13(1)	0.14(1)	0.12(6)	0.06(4)				0.139(7)
	Occ	0.98(4)	0.64(4)	0.55(4)	0.44(4)	0.1(1)				0.89(3)
W2 6*h*	*x/a*	0.261(2)	0.275(3)	0.245(2)	0.235(3)					0.256(2)
	y/b	0.261(2)	0.275(3)	0.245(2)	0.235(3)					0.256(2)
	z/c	0.526(3)	0.514(5)	0.474(3)	0.471(3)					0.525(2)
	U	0.15(2)	0.26(4)	0.13(2)	0.06(2)					0.16(1)
	Occ	0.31(5)	0.48(6)	0.33(4)	0.16(2)					0.46(4)
W3 12*i*	*x/a*	0.170(4)	0.189(8)	0.182(5)	0.173(5)					0.175(3)
	y/b	0.355(7)	0.348(7)	0.334(5)	0.313(5)					0.349(3)
	z/c	0.496(3)	0.448(7)	0.444(3)	0.438(4)					0.499(3)
	U	0.16(1)	0.24(4)	0.20(3)	0.06(2)					0.20(2)
	Occ	0.35(3)	0.21(2)	0.205(3)	0.09(2)					0.35(3)
W4 6*g*	*x/a*	0.364(2)								0.366(2)
	y/b	−0.364(2)								−0.366(2)
	z/c	1/2								0.5
	U	0.22(1)								0.194(1)
	Occ	0.49(3)								0.50(3)
W6 2*c*	*x/a*	0.251(3)	0.287(4)							0.243(2)
	y/b	0.251(3)	0.287(4)							0.243(2)
	z/c	0.251(3)	0.287(4)							0.243(2)
	U	0.13(2)[c]	0.39(2)							0.09(1)
	Occ	0.58(5)	0.31(9)							0.72(7)

[a] Standard deviations are given in parentheses. Multiplicity and Wyckoff letter are reported for each site. U_{eq} (equivalent displacement parameters) values are reported for all framework atoms that were refined anisotropically at all of the investigated temperatures. [b] After the high temperature experiment. [c] Indicates U_{eq} relative to extraframework cations and water molecules refined anisotropically; in all other cases, U_{iso} (isotropic displacement parameters) values are reported.

Table 7. Tetrahedral Bond Distances and Angles and Distortion Parameters at Different Temperatures[a]

		rt	100 °C	125 °C	175 °C	250 °C	300 °C	425 °C	600 °C	rt[b]
T−O1 (Å)	uncorr.	1.6397(8)	1.631(2)	1.630(2)	1.629(2)	1.649(3)	1.651(2)	1.654(2)	1.652(2)	1.6395(8)
	lower	1.646	1.638	1.636	1.635	1.652	1.654	1.657	1.655	1.645
	upper	1.706	1.716	1.719	1.722	1.722	1.723	1.733	1.745	1.702
T−O2 (Å)	uncorr.	1.6445(7)	1.637(2)	1.625(2)	1.617(1)	1.609(1)	1.6112(9)	1.6101(9)	1.609(1)	1.6435(8)
	lower	1.647	1.640	1.629	1.622	1.614	1.615	1.614	1.614	1.646
	upper	1.702	1.711	1.712	1.716	1.705	1.702	1.711	1.729	1.701
T−O3 (Å)	uncorr.	1.6384(6)	1.636(2)	1.629(2)	1.626(2)	1.638(2)	1.634(1)	1.631(1)	1.628(2)	1.6384(7)
	lower	1.642	1.642	1.637	1.633	1.641	1.638	1.635	1.633	1.642
	upper	1.703	1.724	1.733	1.731	1.718	1.712	1.722	1.733	1.701
T−O4 (Å)	uncorr.	1.6429(7)	1.642(2)	1.650(2)	1.660(2)	1.680(2)	1.685(2)	1.689(2)	1.685(2)	1.6425(8)
	lower	1.646	1.647	1.657	1.667	1.683	1.686	1.690	1.686	1.646
	upper	1.700	1.717	1.732	1.747	1.752	1.747	1.755	1.762	1.699
⟨T−O⟩ (Å)	uncorr.	1.6414	1.637	1.634	1.633	1.644	1.645	1.646	1.644	1.6410
	lower	1.645	1.642	1.640	1.639	1.648	1.648	1.649	1.647	1.645
	upper	1.703	1.717	1.724	1.729	1.724	1.721	1.730	1.742	1.701
O3−T−O1 (deg)		111.36(8)	111.8(2)	112.3(2)	112.5(2)	111.9(2)	111.7(1)	111.5(1)	111.6(2)	111.35(9)
O3−T−O2 (deg)		106.27(8)	106.1(2)	107.6(2)	109.0(2)	110.1(2)	110.2(2)	110.5(2)	110.5(2)	106.44(9)
O3−T−O4 (deg)		108.2(1)	106.9(3)	104.6(3)	103.1(3)	106.0(2)	106.2(2)	105.6(2)	105.6(2)	108.1(1)
O2−T−O1 (deg)		107.75(8)	108.1(2)	108.5(2)	109.1(2)	110.0(2)	110.3(1)	110.4(1)	110.3(1)	107.91(9)
O4−T−O2 (deg)		111.3(1)	111.6(2)	112.0(2)	111.7(2)	112.1(3)	112.1(2)	112.3(2)	112.2(2)	111.3(1)
O1−T−O4 (deg)		111.85(9)	112.2(2)	111.7(2)	111.4(2)	106.7(2)	106.3(1)	106.4(1)	106.4(2)	111.6(1)
polyhedral volume (Å^3)		2.265	2.242	2.229	2.225	2.275	2.280	2.283	2.273	2.263
TQE		1.001	1.002	1.002	1.003	1.002	1.002	1.002	1.002	1.001
TAV		5.44	7.40	9.46	11.80	6.74	6.75	7.73	7.49	5.00

[a] Standard deviations are given in parentheses. uncorr., uncorrected distances; lower and upper, lower bound and upper bound distances after correction following Busing and Levy.[40] TQE is the tetrahedral quadratic elongation, whereas TAV is the tetrahedral angle variance according to Robinson et al.[39] [b]After the high temperature experiment.

Table 8. Cation−Oxygen Bond Distances (Å) for CHA Tal N.3 at Different Temperatures[a]

		rt	100 °C	125 °C	175 °C	250 °C	300 °C	425 °C	600 °C	rt[b]
C1	−O4(×6)				2.838(5)	2.473(4)	2.448(3)	2.439(3)	2.459(3)	
C2	−O3(×3)	3.198(5)	3.17(2)	3.062(8)	2.981(7)	3.09(1)	3.07(1)	2.99(1)	2.96(2)	3.192(7)
	−O4(×3)	2.821(4)	2.80(2)	2.604(7)	2.505(6)	2.58(1)	2.54(2)	2.41(2)	2.36(3)	2.818(6)
	−W2	2.86(3)	2.68(2)	2.46(3)	2.59(4)					2.80(2)
	−W3	2.81(2)	3.15(2)	2.44(3)	2.49(4)					2.83(3)
C2a	−O3(×3)		3.07(2)	2.94(2)	2.83(2)					
	−O4(×3)		2.66(2)	2.43(1)	2.26(2)					
	−W2		2.86(2)	2.74(4)	3.11(4)					
	−W3		3.32(2)	2.72(4)	3.01(5)					
C3	−W2	2.31(3)	2.06(4)							2.32(2)
	−W3	2.35(2)	2.44(4)							2.43(3)
	−W4	2.34(2)								2.34(2)
	−W6	2.32(3)								2.42(3)
C4	−O2(×2)	2.83(1)	2.81(1)	3.07(4)						2.84(1)
	−O3	2.55(1)	2.54(2)	2.87(5)						2.57(1)
	−W1	2.35(1)	2.27(2)	2.58(5)						2.34(2)
	−W2	2.80(3)	2.87(2)	3.09(6)						2.90(2)
	−W2	3.05(2)	2.94(1)	3.19(6)						3.08(2)
	−W3	2.39(3)	2.40(1)	2.48(7)						2.27(3)
	−W3	3.09(2)								3.25(3)
C5	−O1(×2)					2.92(2)	2.86(1)	2.85(1)	2.85(1)	
	−O2(×2)					3.22(5)	3.28(1)	3.23(1)	3.24(1)	
	−O3					2.80(8)	2.91(2)	2.87(1)	2.90(2)	

[a] Standard deviations are given in parentheses. [b] After the high temperature experiment.

range for any of the lattice dimensions and consequently of cell volume.

Figure 3 also shows that the whole process is reversible, as revealed by lattice parameters values measured under reversal conditions. Only a slight hysteresis might be noticed in the 100−200 °C temperature range. It is worth noting that, after reversal experiment, diffraction profiles are not as narrow as they are on the untreated crystal (Figure 4); moreover, they become broader and broader after repeated cycles of heating and cooling runs. A general worsening of the crystallinity of the sample is then associated with thermal treatments.

3.3. Crystal Structure at Room Temperature. Structure refinement of data collected at room temperature on the untreated crystal substantially confirms the model proposed in the literature.[15,16] In the natural chabazite used for this study, cations are distributed over three sites (C2, C3, and C4), while water molecules occupy the W1, W2, W3, W4, and W6 positions (see data in Table 6). In detail, for what concerns the cations:

Site C1, located at the center of the six-membered double rings (*d6R* cage), is vacant.

Site C2, along the ternary axis in a peripheral position within the largest cage (the so-called *cha* composite building unit), is partially occupied by K. Cations affinity for this position, as deduced on the basis of the results of Alberti et al., is in fact K < Na ≪ Ca.[15] In this site, cations are coordinated by three oxygen atoms (O4) from framework at

Table 9. Selected Geometrical Parameters Relative to SBUs in Chabazite at Different Temperatures[a]

T (°C)	rt	100 °C	125 °C	175 °C	250 °C	300 °C	425 °C	600 °C	rt[b]
				Six-Membered Double Ring					
O4···O4 (Å)	6.041(4)	6.00(1)	5.78(1)	5.67(1)	4.946(8)	4.898(4)	4.878(4)	4.918(6)	6.030(5)
O3···O4 (Å)	5.24(2)	5.19(5)	5.08(4)	5.03(4)	5.01(7)	5.01(6)	4.99(5)	5.00(6)	5.24(1)
O4−O3−O4 (deg)	101.10(7)	100.7(2)	96.8(2)	96.2(2)	85.0(2)	84.5(1)	84.6(1)	85.7(1)	101.13(9)
O3−O4−O3 (deg)	138.46(8)	138.8(2)	142.2(2)	142.5(2)	144.6(2)	144.4(1)	144.5(1)	144.1(2)	138.38(9)
				Eight-Membered Ring					
O3···O3 (Å)	6.42(5)	6.36(14)	6.41(10)	6.55(14)	6.90(20)	6.97(16)	7.02(13)	7.03(16)	6.43(4)
O2···O2 (Å)	6.94(4)	6.91(11)	6.98(8)	7.04(10)	7.32(13)	7.33(11)	7.33(9)	7.32(11)	6.95(3)
O1···O1 (Å)	6.53(4)	6.54(11)	6.48(9)	6.36(12)	5.69(17)	5.60(14)	5.56(11)	5.56(14)	6.53(4)
O2−O3−O2 (deg)	132.29(6)	132.1(1)	134.9(1)	134.9(1)	143.2(2)	142.7(1)	141.8(1)	141.1(1)	132.31(7)
O3−O2−O1 (deg)	120.36(4)	120.2(1)	119.8(1)	119.5(1)	114.0(1)	113.67(8)	113.78(7)	114.17(8)	120.39(5)
O2−O1−O2 (deg)	141.97(1)	141.18(2)	144.12(2)	147.40(2)	166.30(3)	168.14(3)	168.80(2)	168.33(3)	142.07(1)

[a] Standard deviations are given in parentheses. [b] After the high temperature experiment.

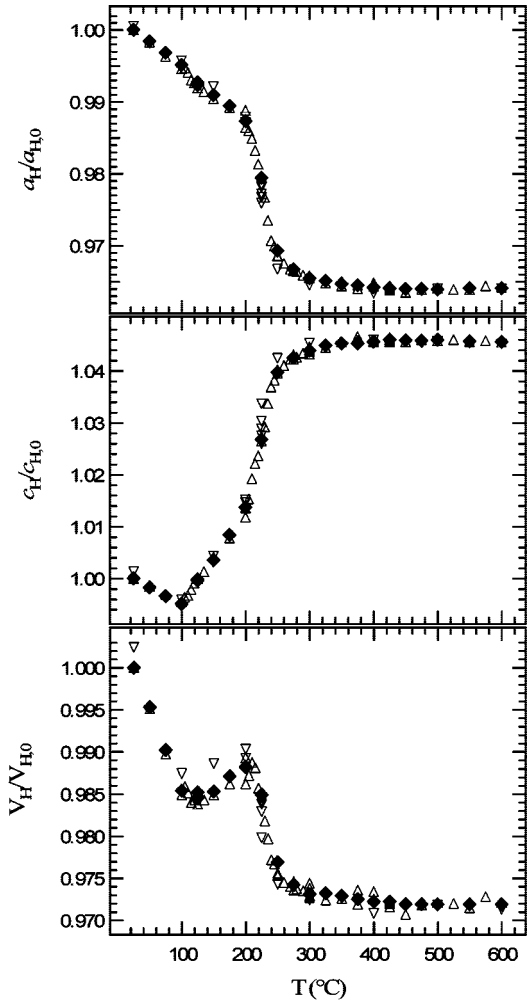

Figure 3. Variations of unit-cell parameters and cell volume (hexagonal setting) with temperature for sample CHA Tal N.3. △, direct experiment; ▽, reversal experiment; ◆, direct measurements by LAT routine (see text).

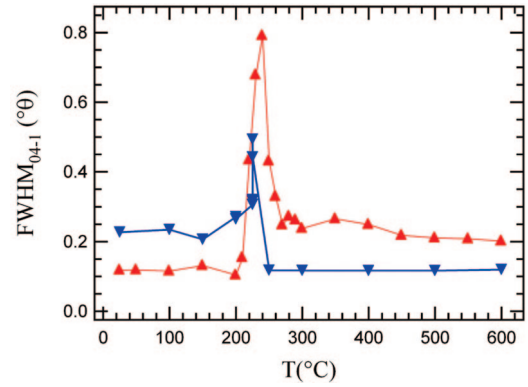

Figure 4. Full width at half-maximum (° θ) of reflection $04\bar{1}$ (hexagonal setting) vs temperature. ▲, direct experiment performed on crystal CHA Tal N.8; ▼, reversal experiment performed on crystal CHA Tal N.3.

ca. 2.8 Å and by W2 and W3 water molecules at 2.81 and 2.86 Å, respectively. Three further oxygen atoms (O3) from the framework are also present in the second coordination sphere of site C2. Refinement of such position happened to be particularly difficult due to the vicinity of the alternative W6 water position (see below).

Site C3, along the ternary axis and within the largest cage, can be regarded as an aquoion. It is in fact coordinated only by water molecules (W2, W3, W4, and W6 are all at ca. 2.3−2.35 Å). Because of the short C3−oxygen distances and the high electron density of the site, Na^+ and Ca^{2+} were allowed to partitionate within the site. According to Alberti et al., there is no strong preference of a given cation for this position, with Na ≈ Ca < K.[15]

Site C4 is also located within the largest cage and shows short distances with two O2 (2.83 Å) and one O3 (2.55 Å) oxygen atoms from the framework. W1, W2, and W3 water molecules are within its coordination sphere as well (2.4−3 Å).

For what concerns the water positions:

W1 position, exactly at the center of the eight-membered ring window, is almost fully occupied in analogy with previous findings.[15,16] It is far from framework oxygen atoms (shortest distances: 3.2 Å) and interpreted as a water molecule also on the basis of its displacement parameter.

W2, W3, and W4 are inside the largest cage, with occupancies ranging between ∼0.3 and 0.5.

W6 is very close to C2; anyway its electron density is high (occupancy 0.6) so it could be refined without the use of constraints in the last cycles of refinement. It has been refined with anisotropic displacement parameters because it has a preferential direction of elongation, which is normal to the ternary axis.

3.4. Crystal Structure Modifications with Temperature. The following analysis of the crystal structure of chabazite as a function of temperature, based on the results of structure refinements from XRD data collected at T = 25, 100, 125, 175, 250, 300, 425, and 600 °C, will consider first the primary building unit (PBU), that is, the Si/Al tetrahedron, second the most relevant geometrical arrange-

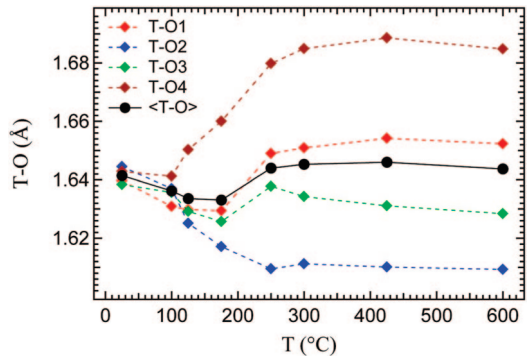

Figure 5. Uncorrected T−O bond distances vs temperature.

ments of tetrahedra in the CHA framework (secondary building units, SBU), and finally extraframework cations and water molecules.

3.4.1. PBU, Primary Building Unit. Uncorrected individual and mean T−O bond distances are plotted in Figure 5 as a function of temperature. The Si/Al tetrahedron does not change significantly in volume in the temperature range investigated, but bond-length distortion increases significantly. In fact, while at room temperature all tetrahedral individual distances are very similar, ranging between 1.6384(6) and 1.6445(7) Å, at $T = 600$ °C they are spread over a wider range, between 1.609(1) and 1.685(2) Å. The increasing tetrahedral internal distortion with temperature is also confirmed by the variation of tetrahedral angle variance (TAV),[39] which increases linearly from 5.44 at room temperature to 11.80 at 175 °C, and then remains almost constant at a value of ∼7 at $T > 200$ °C (see data in Table 7). Changes in the dimensions of the individual T−O bond lengths and T−O−T linkages of the tetrahedra with temperature have also been found for pure siliceous chabazite.[17,19]

The T−O average distance remains then nearly the same with temperature, but, while T−O1 and T−O3 stay approximately constant, the T−O4 distance increases and the T−O2 distance decreases significantly with temperature. To make the changes within the framework plain, it is worth analyzing the different T−O distances in terms of the bonds formed by the oxygen atoms from framework with extraframework cations, as will be discussed below. For the present discussion, it should be considered that O4 atoms form part of the coordination environment of the cationic site C2 whose occupancy increases with T up to 200 °C, thus weakening slightly the T−O4 bond and lengthening the T−O4 distance. At higher temperature and up to 600 °C, C2 sites are vacant and O4 atoms are involved in the coordination of the C1 position at the center of the *d6R* unit. On the other hand, at room temperature O2 participates in the coordination environment of the C4 sites, whose occupancy decreases rapidly and is nil at 125 °C, thus reinforcing the T−O2 bond whose distance, as a consequence, decreases significantly in this T range. At higher temperatures, no significant further changes occur to the T−O2 bond distance because O2 atoms are only loosely coordinated to C5 cations.

It is well-known from the literature that the interatomic distances measured by XRD are typically underestimated and appropriate corrections, which imply the use of accurate estimates of anisotropic displacement parameters (ADPs), should be applied. To perform the correction for thermal motion in a general case, it is necessary to know, in addition to the ADPs, the correlation tensors between the displacement of the bonded atoms, which cannot be directly deduced from Bragg diffraction measurements, but in principle can be obtained by lattice dynamical calculations. Nonetheless, without assuming any specific model for vibration (e.g., rigid body, riding or uncorrelated motion, etc.), bond distances cannot be corrected for thermal motion. In these cases, only an estimate of the possible errors, that is, an upper and a lower limit for the corrected interatomic distances, can be obtained.[40−43] Such values are reported in Table 7 for the studied chabazite. Even within the limits of these correction, the observed variations discussed above, that is, a differentiation of the four T−O distances, are still evident. At any rate, a rigid-body test[44] based on the assumption that along the bond direction the mean-square displacements of chemically bonded atoms should be essentially the same, due to the difficulty of stretching the bond,[45,46] has been applied. Defined Δ, the difference between the mean square displacement (MSQD) of O and Si along the bond, the Si−O bond can be considered rigid if $0.00125 < \Delta < 0.002$ Å^2.[45] The chabazite of this study does not meet this criterion showing at room temperature a $\Delta = 0.0045$ Å^2 with esd = 0.00036 Å^2, thus indicating a substantially disordered distribution of Si and Al. Few zeolites satisfy the rigid-bond criterion and are mainly those considered ordered.[45] With increasing temperature, the Δ values of the analyzed chabazite remain approximately constant and also after dehydration $\Delta = 0.0037$ Å^2 (esd = 0.00066 Å^2).

3.4.2. SBU, Secondary Building Units. The evolutions with increasing temperature of the six-membered double ring (*d6R*) and the eight-membered ring are displayed in Figures 6 and 7, respectively. At room temperature, the two six-membered rings forming the former SBU are almost eclipsed and the individual rings show an internal O4−O3−O4 angle of ∼101°. With increasing temperature, tetrahedra rotate around the Si−Si axle defined between two overlapping tetrahedra along the 3-fold axis, and the rings become more distorted (O4−O3−O4 angle approaching ∼84°). The decrease of the O4−O3−O4 angle together with the expansion of the Si−O4 bond length produces a narrowing of the channels as the adjacent Si atoms belonging to the same ring move closer together. This is responsible for the contraction of the a_H dimension. Furthermore, the rotation of the tetrahedra around the Si−Si axle pulls the two six-membered rings closer together as revealed by the decrease of the Si−Si distance from 3.137(1) to 2.946(2) Å and of the bridging Si−O1−Si angle from 146.1(2)° to 126.3(2)° between room

(41) Johnson, C. K. Generalized treatments for thermal motion. In *Thermal Neutron Diffraction*; Willis, B. T. M., Ed.; Oxford University Press: Oxford, UK, 1970; pp 132−160.
(42) Johnson, C. K. An introduction to thermal motion analysis. In *Crystallographic Computing*; Ahmed, F. R., Ed.; Munksgaard: Copenhagen, Denmark, 1970; pp 220−226.
(43) Scheringer, C. *Acta Crystallogr., Sect. A* **1972**, *28*, 616.
(44) Hirshfeld, F. L. *Acta Crystallogr., Sect. A* **1976**, *32*, 239.
(45) Downs, R. T.; Gibbs, G. V., Jr. *Am. Mineral.* **1990**, *75*, 1253.
(46) Willis, B. T. M.; Pryor, A. W. *Thermal Vibrations in Crystallography*; Cambridge University Press: Cambridge, UK, 1975.

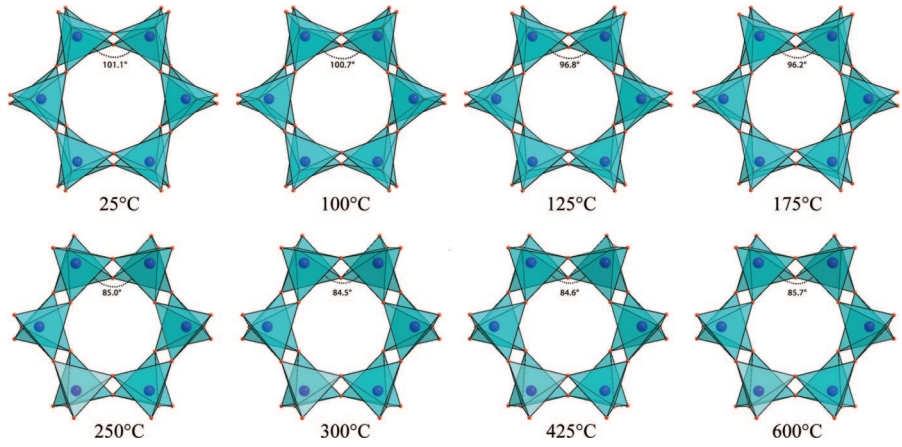

Figure 6. The six-membered double ring from room temperature to 600 °C viewed normal to c_H.

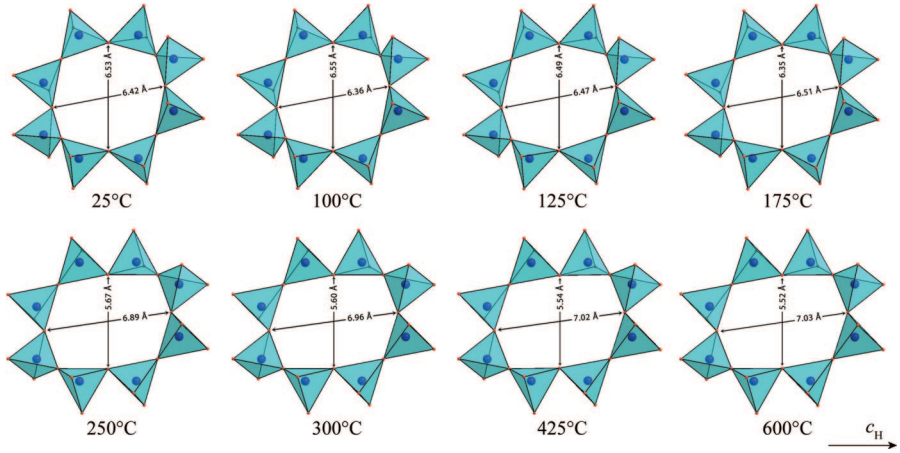

Figure 7. The eight-membered ring from room temperature to 600 °C.

temperature and 300 °C. The net effect induced is of increasing the O3···O3 distance and decreasing the O1···O1 distance in the eight-membered ring. In Figure 7, it is in fact evident how the eight-membered ring becomes shorter along a_H and more elongated in the c_H direction, thus lengthening the c_H dimension as temperature increases. In both cases, the structural modifications are almost complete at 250 °C, and no significant further variations occur at higher temperatures.

3.4.3. Extraframework Cations and Water Molecules. Cation site occupancies as a function of temperature are reported in Figure 8; the crystal structures of chabazite at room temperature, 175 °C, and 600 °C are compared in Figure 9.

As discussed above, at room temperature cations occupy the C2 and C4 sites, in which they are partly coordinated by oxygen atoms of the framework and partly by extraframework water molecules, and the C3 site where they form aquoions being surrounded exclusively by water molecules. All of these positions are located within the largest cage of the chabazite framework, as displayed in Figure 9a.

The first evident feature occurring as temperature is increased is the breakdown of the Ca and Na aquoions. At 100 °C in fact the C3 position is already almost vacant (only 2 residuals electrons out of 14 present at room temperature), and it is completely vacant at 125 °C. The first water molecules to be lost are in fact those located at site W4,

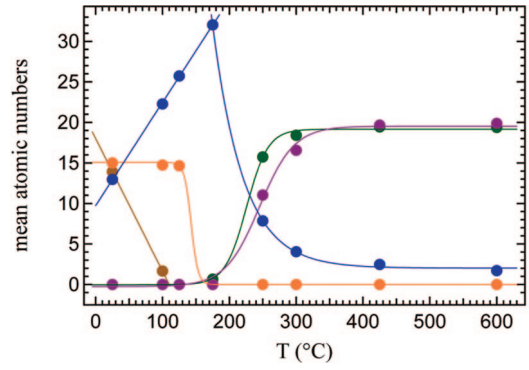

Figure 8. Mean atomic numbers at cationic sites vs temperature. Site C1, green; site C2 (C2 + C2a), blue; site C3, brown; site C4, orange; site C5, purple. For visual purposes, sigmoid fits are reported for sites C1, C4, and C5; C2 occupancy has been fitted linearly from room temperature to 175 °C ($R^2 = 0.9999$) and exponentially from 175 to 600 °C ($\chi^2 = 0.198$); C3 occupancy decreases linearly from room temperature to 100 °C and is nil at higher temperatures.

involved exclusively in the coordination of C3 cations. Such cations migrate then toward C2, which in turn now hosts three different species (K^+, Na^+, and Ca^{2+}) characterized by different ionic radii. As a consequence, starting from 100 °C, this site is characterized by positional disorder with electron density significantly elongated in the c_H direction. A split position named C2a could be refined to account for the increased electron density at the site. At $T = 175$ °C,

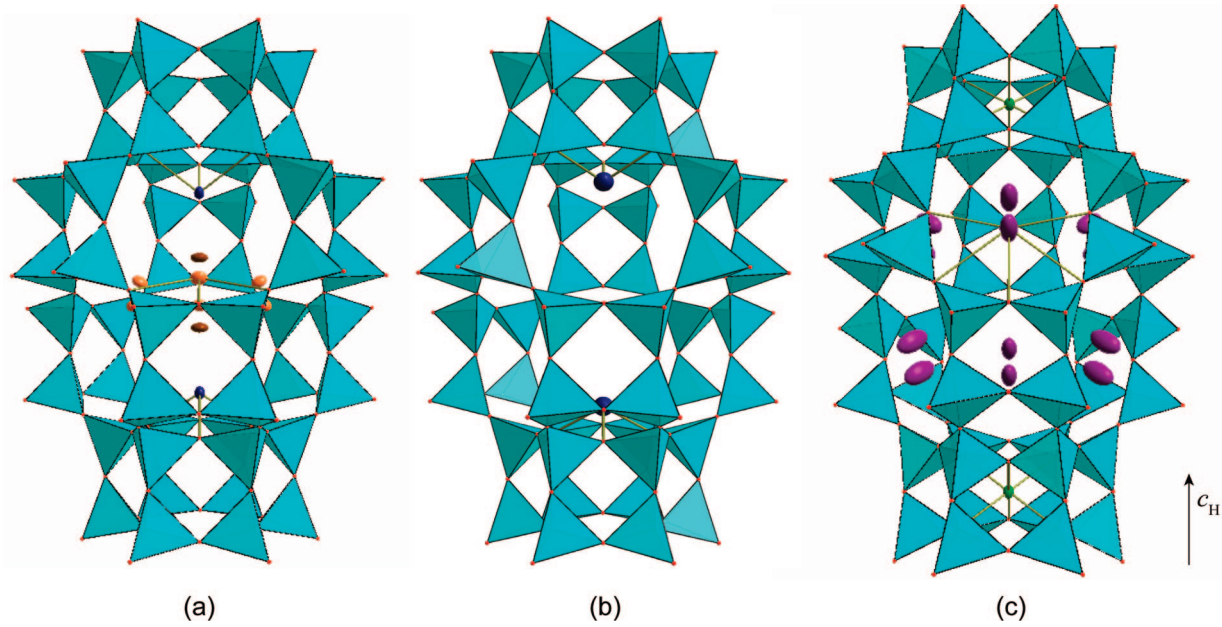

Figure 9. Crystal structure of chabazite at (a) 25 °C, (b) 175 °C, and (c) 600 °C. Cation sites, including symmetrically equivalent positions, are reported. Symbols are of the same colors as in Figure 8. At $T = 25$ °C cations occupy the C2 (blue), C3 (brown), and C4 (orange) sites, at $T = 175$ °C all cations are in C2 (split along c_H not displayed), whereas at $T = 600$ °C cations are in C1 (green) and C5 (purple) sites. Bonds with oxygen atoms from framework are reported. The six equivalent C4 sites at room temperature as well as the two equivalent C5 positions within the same eight-membered ring at 600 °C are of course alternative; in these cases only bonds relative to one position are displayed.

due to the decreased hydration degree, also the C4 site becomes unstable and is found to be vacant. All of the cations are now located at the C2/C2a site as shown in Figure 9b where the crystal structure of chabazite at 175 °C is reported. At this temperature, the overall number of electrons refined at the cationic sites is fairly lower than that obtained from data collected at lower temperatures. This might be rationalized in terms of cationic mobility, as already suggested by Smith et al.[23] It is worth noting that the number of electrons is still relatively low at 250 °C and returns to its normal value at higher temperatures.

A sudden change in the direction of cation migration occurs then when temperature is further increased. Results of structure refinements reveal in fact that at $T \geq 250$ °C also the C2 site is unstable due to the loss of the water molecules participating in its coordination sphere. Therefore, cations start migrating toward smaller cavities where coordination is assured by oxygen atoms of the framework only. In particular, cations move toward the six-membered double ring (C1 site), where they are in octahedral coordination with cation−oxygen distances of ∼2.45 Å, and toward a peripheral position within the eight-membered ring, which was labeled as C5. The former position corresponds to the Ca1 site reported by Smith et al.[23] in dehydrated Ca-chabazite and confirmed by Mortier et al.[24] and Butikova et al.[25] The latter cationic site has the same topology of the III4 site found by Mortier et al.[26] in dehydrated Na-exchanged chabazite. It shows a planar configuration, and the cation first coordination sphere includes five oxygen atoms of the ring at distances ranging between ∼2.9 and ∼3.2 Å. Because of the large dimension of the cavity, K^+ ions (plus small amounts of Na^+ ions) were refined on this position, while Na^+ and Ca^{2+} were allowed to partitionate on C1. These two positions are stable up to 600 °C, and their geometries do not change significantly in the 250−600 °C temperature range.

Reversal experiments demonstrate that the whole process is reversible under the conditions of this study; by decreasing temperature, water enters the structure again and cations migrate back to their original positions.

4. Conclusions

In the room temperature to 700 °C temperature range, natural chabazite undergoes two net discontinuities at $T =$ 100 °C and $T = 200$ °C, both implying a change in the direction of cell volume variation vs temperature. Structure refinements confirm that no symmetry change is associated with these discontinuities. It is worth noting that the second discontinuity occurs, in concomitance with the beginning of peaks broadening, when the hydration degree of the sample is ca. 4 H_2O mol per unit-cell, very close to the value where a phase transition is expected from thermochemical data.[28,29] Also, an important change in the thermal evolution of the natural chabazite under investigation occurs at temperatures higher than 300 °C when migration of cations toward C1 and C5, which starts after the second discontinuity, is over, and cell volume results to be almost constant up to 700 °C. Such features in the thermal evolution of unit-cell volumes in chabazite reflect the progressive loss of water molecules from different crystallographic sites and confirm the presence of energetically distinct types of H_2O as revealed by Fialips et al.[30]

It is worth noting that migration of all of the extraframework cations from C2 toward C1 and C5 could account for the broadening of diffraction profiles observed in the temperature range 200−250 °C. Furthermore, no significant

chemical variations occur at temperatures above ~300 °C because the system can be considered already anhydrous within the limits of the measurements, and no crystallographic variations occur either, because cations have already reached their final positions on C1 and C5 sites. Unit-cell variations measured in the range 300−700 °C account then for thermal expansion of the natural chabazite under investigation, which results to be almost nil. The observed behavior is different from that of pure siliceous chabazite, which shows negative expansion in this range[18,19] and might be rationalized considering that SBUs are not allowed to contract by rotation of tetrahedra because they must maintain a suitable environment for the coordination of cations.

Cations act in fact as template agents for the chabazite channel. As long as water content is enough to guarantee a suitable coordination sphere for all of the cations, these distribute all inside the largest cage and the channel takes a relatively "short and fat" conformation. At room temperature in fact the *d*6*R* cavity is too large to host any cation and also the eight-membered ring assumes an almost circular shape not suitable for cation coordination. Upon dehydration, cations move inside these cavities, which adapts their shape accordingly. The two rings forming the *d*6*R* cage twist so that they can move close together and form a regular octahedron where Na^+ and Ca^{2+} can be hosted, whereas the eight-membered ring assumes a more ellipsoidal shape so that cations can find a suitable number of ligands by adopting a peripheral position within the ring. The net effect of such deformations is that the channel of chabazite at high temperature takes a relatively "tall and slim" conformation. Modifications of the framework are associated with an internal deformation of the tetrahedron itself. T−O bond lengths are in fact sensible to the variable chemical environments of the oxygen atoms, which may or may not be involved in the coordination of extraframework cations. Our results enabled then to observe the influence of different chemical bonding on the framework.

Acknowledgment. We thank P. Ghigna for TG analysis, R. Gastoni for sample preparation, and S. Bigi for electron microprobe analyses. This manuscript benefited from the suggestions of one anonymous reviewer.

CM800781T